

## Modeling detailed sedimentary $^{210}\text{Pb}$ and fallout $^{239,240}\text{Pu}$ profiles to allow episodic events: An application in Chesapeake Bay

Yonghong Nie,<sup>1</sup> Ismail B. Suayah, and Larry K. Benninger

Department of Geological Sciences, University of North Carolina, Chapel Hill, North Carolina 27599-3315

Marc J. Alperin

Department of Marine Sciences, University of North Carolina, Chapel Hill, North Carolina 27599-3300

### Abstract

Dependable sediment chronologies are essential to the interpretation of the sedimentary record of past environmental change. In the present article, we use high-resolution chemical and radiochemical data as the basis for a numerical simulation of sediment accumulation, bioturbation, and episodic deposition or erosion in a dynamic estuary. We simulate episodic events by employing a time dependent sedimentation rate that we solve by finding a set of model parameters that describes depth profiles of both excess  $^{210}\text{Pb}$  and fallout  $^{239,240}\text{Pu}$ . We apply the model to depth distributions of these tracer nuclides in cores from upper-, mid- and lower-Bay sites in Chesapeake Bay. At the upper-Bay site, combining chemical and radiochemical data permits us to recognize and to quantify the sediment deposition due to tropical storm Agnes (1972). At the lower-Bay site, we demonstrate nonsteady sedimentation and propose plausible scenarios to account for it. Given adequate data, our model can provide information that is not available from steady-state models.

An accurate retrospective analysis of nutrient or pollutant input based on sediment stratigraphy requires detailed information regarding sedimentation rates. The most widely used methods for quantifying modern (past 10–100 yr) sediment accumulation are based on vertical distributions of particle tracers such as excess (xs)  $^{210}\text{Pb}$  and fallout  $^{137}\text{Cs}$  and  $^{239,240}\text{Pu}$  (e.g., Officer et al. 1984; Appleby and Oldfield 1992). Sediment accumulation rates can be inferred from depth profiles of these tracers, provided that the influx of tracer, mixing rate, and mixing depth are known. The rate and depth of sediment mixing are important for determining sedimentation rates because mixing dilutes the surficial activity of steady-state tracers and diffuses the stratigraphic signal of time-dependent tracers (e.g., Benninger et al. 1979).

Interpretation of tracer distributions from estuarine sediments may be complicated by the occurrence of episodic events. Dramatic increases in particle loading and bottom currents associated with hurricanes and major storms can result in massive sediment accumulation or resuspension and erosion. Although the frequency of such events is low, the quantity of material deposited or eroded may be sufficient to have a significant impact on the vertical distribution of tracers.

Because tracer distributions in estuarine sediments are affected by numerous processes (e.g., particle deposition, benthic mixing, and storm events), multiple tracers are neces-

sary to effectively constrain sedimentation rates. Tracers with distinct input functions provide independent information that can be used to deconvolve long-term accumulation, episodic deposition or erosion, and sediment mixing. The combination of xs  $^{210}\text{Pb}$  and fallout isotopes is well suited for this purpose: atmospheric deposition of xs  $^{210}\text{Pb}$  is nearly steady-state (Appleby and Oldfield 1992); whereas deposition of fallout nuclides is highly time-dependent (HASL 1977; Larsen 1985). Coupling the two tracers should provide a much tighter constraint on sedimentation and mixing rates than either tracer considered individually.

The objective of this study is to evaluate the effectiveness of coupling high-resolution profiles of xs  $^{210}\text{Pb}$  and fallout nuclides in order to constrain sedimentation rates in a dynamic estuary subject to bioturbation and major storm events. We chose Chesapeake Bay as our working site because it has been the focus of numerous sediment-based retrospective studies (e.g., Goldberg et al. 1978; Cornwell et al. 1996; Cronin et al. 1999) and has been affected by major flood events during the past century, including tropical storm Agnes, which hit the region in 1972. Several studies have presented evidence for episodic deposition in the northern portion of Chesapeake Bay (Schubel and Zabawa 1977; Hirschberg and Schubel 1979; Helz et al. 1985/1986). Analyses of sediment cores collected from the upper reaches of the Bay after passage of tropical storm Agnes in 1972 show that the storm left a sediment layer ranging in thickness from 4 to 20 cm (Schubel and Zabawa 1977). To the best of our knowledge, no effects of flood or storm events have been recognized in sediments of the lower Bay.

### Methods

*Sample collection*—Box cores were collected from the RV *Gyre* during 30 June and 1 July 1994. Locations of the coring sites are shown in Fig. 1. Water depths at the upper-Bay

<sup>1</sup> Corresponding author (ynie@isis.unc.edu).

### Acknowledgments

We would like to thank the crew of the R/V *Gyre* for their assistance in sampling and Kent Ratajeski, who helped us with DCP analyses. We also thank three anonymous reviewers for their helpful comments. Support for this research came from the Martin McCarthy fellowship in Department of Geological Sciences, University of North Carolina at Chapel Hill, and Department of Energy through grant DE FG05 92ER61413.

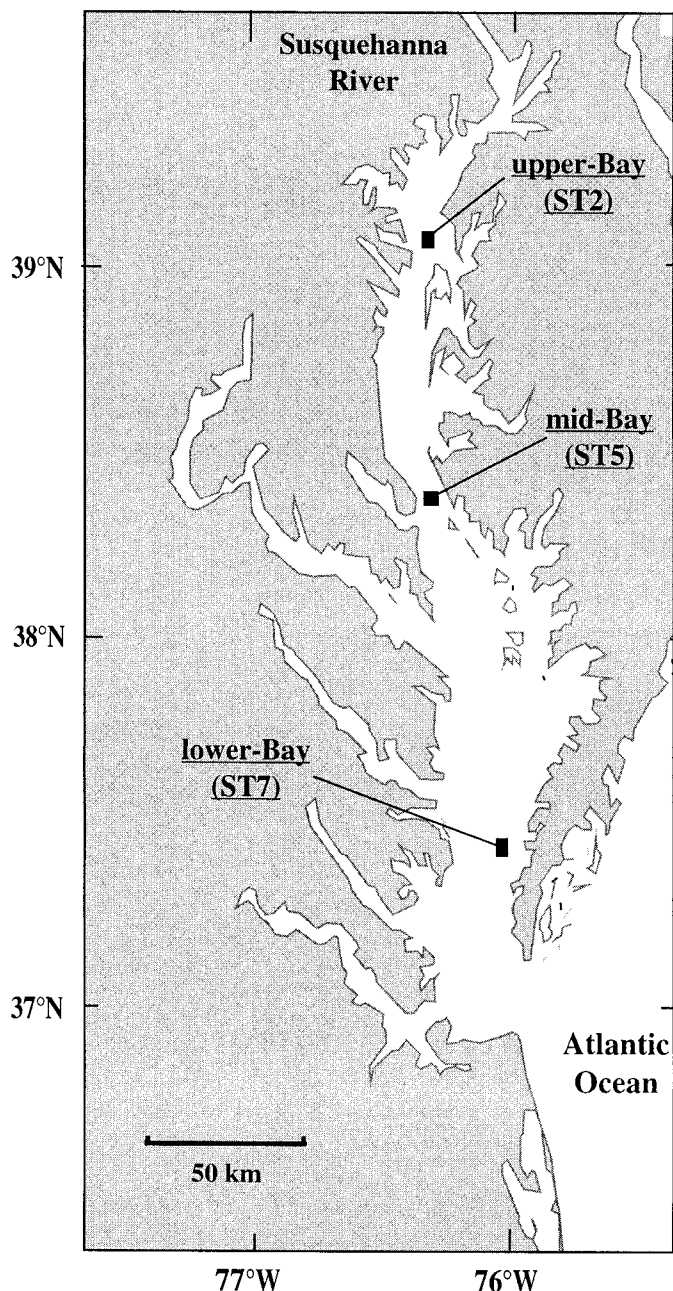


Fig. 1. Map of Chesapeake Bay region showing the three sampling sites: upper-Bay (ST2 at 39°06.158'N, 76°19.997'W), mid-Bay (ST5 at 38°22.049'N, 76°19.951'W), and lower-Bay (ST7 at 37°24.038'N, 76°05.184'W).

(ST2), mid-Bay (ST5) and lower-Bay (ST7) stations were 6.5, 21, and 15 m, respectively. Two subcores (9.5 cm diameter) were taken from each box core, and sediments from 1-inch (2.54 cm) intervals from the two subcores were combined for the analyses reported here. Below the top two samples (~5 cm), sediment in contact with the inner wall of the core tube was discarded.

**Wet chemistry**—Sediment samples were dried at 100°C, and porosity was calculated from mass percent water. Loss-on-ignition (LOI) was determined on a subsample of dry

sediment by roasting in air for 2 d at 475°C. Most of the remaining dry sediment was packed into Erlenmeyer flasks for gamma spectrometry on an intrinsic Ge detector (Benninger and Wells 1993).  $^{137}\text{Cs}$  was considered finite when peak area exceeded baseline by at least 2 SD; otherwise, it is reported as not detected (ND). All  $^{137}\text{Cs}$  activities were decay corrected to the date of core collection.  $^{226}\text{Ra}$  activities were determined from daughter nuclides  $^{214}\text{Pb}$  (295 and 352 keV) and  $^{214}\text{Bi}$  (609 keV).

$^{210}\text{Pb}$  and  $^{239,240}\text{Pu}$  were determined by alpha spectrometry after acid digestions of samples (Benninger and Wells 1993). For  $^{210}\text{Pb}$ , 1–1.5-g samples were spiked with  $^{209}\text{Po}$  and totally dissolved by microwave heating. Excess  $^{210}\text{Pb}$  is total  $^{210}\text{Pb}$  minus  $^{226}\text{Ra}$ , decay-corrected to the date of core collection. Because xs  $^{210}\text{Pb}$  in surficial sediments is underestimated because of  $^{222}\text{Rn}$  loss (Key et al. 1979; Martens et al. 1980; Imboden and Stiller 1982), we have corrected for this effect using the method of Imboden and Stiller (1982). We assume a Rn diffusivity of  $8 \times 10^{-6} \text{ cm}^2 \text{ s}^{-1}$  (Imboden and Stiller 1982) and that 60% of the  $^{222}\text{Rn}$  produced by  $^{226}\text{Ra}$  decay escapes into pore water. We show both corrected and uncorrected data below. Our modeling is based on the corrected xs  $^{210}\text{Pb}$  data. For the Pu analysis, ~10 g of dry sediment was spiked with  $^{242}\text{Pu}$  and leached for 7 h in hot  $\text{HNO}_3$  (~15 M). Pu was separated by anion-exchange chromatography (Anderson and Fleer 1982) and electrodeposited on stainless steel disks (Kressin 1977) for alpha spectrometry.

For major-element chemistry, aliquots of ashed sediment were fused with Li metaborate or metaborate/tetraborate fluxes and dissolved in dilute  $\text{HNO}_3$ . K was measured by direct-coupled plasma spectrometry following procedures outlined in Klein et al. (1991). Fe and Si were determined by visible spectrophotometry by use of the single-solution procedure of Shapiro (1975). Analyses were standardized against well-characterized rock and sediment reference materials (Gladney and Roelandts 1988).

**Sediment mixing model**—In this section, we describe a diffusion-advection-reaction model for xs  $^{210}\text{Pb}$  and  $^{239,240}\text{Pu}$  in sediments. The model will allow us to evaluate sedimentation and mixing rates that are consistent with tracer profiles at the three study sites in the Chesapeake Bay.

Similar to other sediment numerical models (e.g., Officer 1982; Lynch and Officer 1984; Christensen and Bhunia 1986; Robbins 1986), our model assumes that sedimentation and bioturbation are the major processes that affect the distribution of particle-reactive tracers in the sediment column. However, our modeling approach has two significant modifications. First, we have relaxed the requirement of uniform sedimentation rate to allow for time-dependent sedimentation. Others have noticed episodic deposition in estuarine sediment (Schubel and Zabawa 1977; Hirschberg and Schubel 1979; Helz et al. 1985/1986; Sugai et al. 1994). However, to the best of our knowledge, the effort to distinguish this effect has previously been limited to cutting a certain portion from the tracer profile and modeling the event-corrected profile with a steady-state model (Goldberg et al. 1978; Sugai et al. 1994). The novel approach described here is an extension of the existing steady-state models and gives the flexibility to simulate episodic deposition or erosion that may

have occurred in association with major storm events. Second, we optimize sedimentation and mixing rates by finding a set of parameters that fit both the  $^{210}\text{Pb}$  and  $^{239,240}\text{Pu}$  data. Compared with modeling the  $^{210}\text{Pb}$  and fallout data separately, our approach yields tighter constraints on the sediment-transport parameters.

One of the pitfalls with nonsteady models is that one can envision an infinite number of ways that sedimentation rates might have changed during the past  $\sim 100$  yr (the time period covered by xs  $^{210}\text{Pb}$  and fallout radionuclides). Following a practice that is common in modeling studies (e.g., Boudreau and Ruddick 1991), our strategy is to use the simplest sedimentation rate scenario that recreates the essential features of both the xs  $^{210}\text{Pb}$  and  $^{239,240}\text{Pu}$  depth distributions and conforms to observed patterns in sediment lithology. Thus, our initial simulations assume a constant sedimentation rate. If this fails to account for pronounced features in one or more sediment profiles, we adopt the simplest nonsteady scenario: constant sedimentation rate punctuated by an event (rapid deposition or erosion) that we simulate as an abrupt change in sedimentation rate over a short period of time. This approach is most plausible when the event can be linked to a specific storm. If this scenario does not produce an acceptable simulation, our next approach is to assume that the storm had a long-term impact on sediment supply, resulting in different deposition rates before and after the event. Additional complexity in the sedimentation rate scenario is not needed to accurately simulate profiles at our 3 study sites (see below).

Depth distributions of xs  $^{210}\text{Pb}$  and  $^{239,240}\text{Pu}$  can be described by an equation that includes terms that account for bioturbation, variable sediment advection, compaction, and radioactive decay (Officer and Lynch 1982):

$$\frac{\partial[(1-\phi)\rho C]}{\partial t} = \frac{\partial\left[(1-\phi)\rho D_B \frac{\partial C}{\partial x}\right]}{\partial x} - \frac{\partial[(1-\phi)\rho\omega' C]}{\partial x} - (1-\phi)\rho\lambda C, \quad (1)$$

where  $D_B$  ( $\text{cm}^2 \text{yr}^{-1}$ ) is the bioturbation coefficient,  $\omega'$  ( $\text{cm yr}^{-1}$ ) is the time-dependent sedimentation rate,  $x$  (cm) is sediment depth,  $t$  (yr) is time,  $\phi$  is sediment porosity,  $\rho$  is density of the sediment solid phase ( $2.5 \text{ g cm}^{-3}$ ),  $C$  ( $\text{mBq g}^{-1}$ ) is the activity of radionuclide (xs  $^{210}\text{Pb}$  or  $^{239,240}\text{Pu}$ ), and  $\lambda$  denotes the decay constant ( $\lambda = 0.031 \text{ yr}^{-1}$  for  $^{210}\text{Pb}$  and  $\sim 0$  for  $^{239}\text{Pu}$  and  $^{240}\text{Pu}$ ). Implicit in Eq. 1 are the assumptions that (1)  $^{210}\text{Pb}$  and  $^{239,240}\text{Pu}$  are irreversibly bound to particles, (2) bioturbation can be represented as a diffusive process, and (3) mixing of  $^{210}\text{Pb}$  and  $^{239,240}\text{Pu}$  can be simulated by the same  $D_B$  value.

Compaction is simulated by decreasing porosity exponentially with depth:

$$\phi = (\phi_0 - \phi_\infty)\exp(-\beta x) + \phi_\infty, \quad (2)$$

where  $\phi_0$  is the porosity at sediment-water interface,  $\phi_\infty$  is porosity at infinite depth, and  $\beta$  is the scale-length coefficient. Values for porosity parameters ( $\phi_0$ ,  $\phi_\infty$ ,  $\beta$ ) are derived by fitting Eq. 2 to measured porosity-depth distributions. Porosity is assumed to be at steady state, and no attempt is

made to account for discontinuities in porosity profiles. This assumption is crucial for keeping the equations reasonably simple. Porosity gradients are treated by use of the ‘‘intra-phase mixing’’ model (Mulsow et al. 1998), which implies that porosity is independent of bioturbation rates. The decrease in sedimentation rate with depth, due to compaction, is given by

$$\omega' = \omega'_\infty \frac{(1 - \phi_\infty)}{(1 - \phi)}, \quad (3)$$

where the subscript ( $\infty$ ) denotes values at infinite sediment depth.

Depth-dependence of the mixing coefficient ( $D_B$ ) is described by the complementary error function (erfc) (Robbins 1986):

$$D_B = \frac{D_{B_0}}{2} \text{erfc}\left(\frac{x - x^*}{\sigma}\right), \quad (4)$$

where  $D_{B_0}$  is the bioturbation coefficient at sediment-water interface,  $x^*$  is the depth where  $D_B/D_{B_0} = 0.5$ , and  $\sigma$  is a constant that controls  $dD_B/dx$  in the vicinity of  $x = x^*$ . Setting  $\sigma = 2$  results in a relatively rapid decline in  $D_B$  at the base of the mixed layer. Because  $D_B$  decreases to 0 only at infinite depth, it is useful to define a sediment depth over which the effects of bioturbation are measurable. Similar to Robbins (1986), we define the mixed layer depth as the depth at which  $D_B$  is 10% of its value at the surface. This model is a continuous equivalent of the traditional, simple two-layer mixing model that allows  $D_B$  to decrease continuously through the bottom of the mixed layer. The continuity of  $D_B$  is necessary for the stability of the numerical solution, and is also reasonable because one can envision that bioturbation would not stop suddenly at a certain depth but would decrease continuously with depth. Robbins (1986) used half-Gaussian and erfc to simulate the depth dependence of the bulk diffusivity associated with both diffuser species and advector species. Substituting the half-Gaussian for erfc has a negligible affect on our results.

Solving Eq. 1 requires specifying upper and lower boundary conditions and defining the initial profile (i.e., the radionuclide depth-distribution at  $t = 0$ ). The upper boundary condition is given by the influx of tracer at the sediment surface ( $F'_0$ ):

$$F'_0 = (1 - \phi_0)\rho\omega'_0 C_0 - D_{B_0}(1 - \phi_0)\rho\left(\frac{\partial C}{\partial x}\right)_0, \quad (5)$$

where the subscript (0) denotes values at the sediment-water interface and the superscript ( $t$ ) indicates that a parameter may be time-dependent.

Atmospheric deposition of xs  $^{210}\text{Pb}$  at a single location is generally considered to be steady when averaged over several years (Appleby and Oldfield 1992). For the steady sedimentation  $^{210}\text{Pb}$  model, the upper boundary influx ( $F_0[\text{Pb}]$ ) is set equal to the product of the decay constant and sediment inventory:

$$F_0[\text{Pb}] = \lambda\rho \int_0^\infty C(1 - \phi) dx. \quad (6)$$

For sediment cores having finite xs  $^{210}\text{Pb}$  activity in the deepest samples, total inventories are estimated by extrapolating the measured profiles to zero activity assuming constant sediment accumulation.

For modeling episodic deposition, we assume that prior to the event, the influx of xs  $^{210}\text{Pb}$  ( $F_0^{\text{pre}}[\text{Pb}]$ ) and sedimentation rate ( $\omega_z^{\text{pre}}$ ) are constant. Because the sedimentation rate during the event is very different from  $\omega_z^{\text{pre}}$ , the xs  $^{210}\text{Pb}$  influx during the event probably is different from the normal influx. The influx after the event also might be different from that before the event if the episodic event has a long-term effect on the regional sediment distribution. The effect of changes in sedimentation rate on the input flux of xs  $^{210}\text{Pb}$  depends on the relationship between the transfer function ( $\Phi_{\text{pb}}$ , the ratio of atmospheric  $^{210}\text{Pb}$  flux to sediment  $^{210}\text{Pb}$  flux) and sedimentation rate. There are two end-member models that describe this relationship (Appleby and Oldfield 1992). The first assumes that  $\Phi_{\text{pb}}$  is constant, implying that the influx of  $^{210}\text{Pb}$  is not affected by the change in sedimentation rate. The second assumes that  $\Phi_{\text{pb}}$  is directly proportional to the mass flux, implying that the  $^{210}\text{Pb}$  influx increases or decreases in proportion to sedimentation rate. In most environments, the relationship between  $\Phi_{\text{pb}}$  and  $\omega_z$  will fall between the two extreme models. To allow for intermediate cases, we introduce an adjustable transfer function parameter for xs  $^{210}\text{Pb}$  ( $P_{\text{pb}}$ ) which can vary from 1 (constant  $\Phi_{\text{pb}}$ ) to 0 ( $\Phi_{\text{pb}} \propto \omega_z$ ). Thus, the time-dependent influx of xs  $^{210}\text{Pb}$  ( $F_0^t[\text{Pb}]$ ) is

$$F_0^t[\text{Pb}] = \begin{cases} F_0^{\text{pre}}[\text{Pb}] & t_0 < t < t_{\text{event}} \\ F_0^{\text{pre}}[\text{Pb}] \cdot [P_{\text{pb}}^{\text{event}} + (1 - P_{\text{pb}}^{\text{event}}) \times \omega_z^{\text{event}}/\omega_z^{\text{pre}}] & t_{\text{event}} < t < t_{\text{event}} + 0.1 \\ F_0^{\text{pre}}[\text{Pb}] \cdot [P_{\text{pb}}^{\text{post}} + (1 - P_{\text{pb}}^{\text{post}}) \times \omega_z^{\text{post}}/\omega_z^{\text{pre}}] & t_{\text{event}} + 0.1 < t < t_c \end{cases} \quad (7)$$

where “event” and “post” denote  $P_{\text{pb}}$  values and sedimentation rate during and after the event, respectively,  $t_0$  is the time when the simulation begins,  $t_{\text{event}}$  is the time corresponding to the episodic deposition (0.1 yr is the assumed duration of the event), and  $t_c$  is the time when the sediment core was collected. We then solve for  $F_0^{\text{pre}}[\text{Pb}]$  by integrating the decay-corrected input flux and forcing mass balance with the sediment inventory:

$$\int_{t_0}^{t_c} F_0^t[\text{Pb}] \exp[-\lambda(t_c - t)] dt = \rho \int_0^\infty C(1 - \phi) dx. \quad (8)$$

In a real situation, the event influx is not simply dependent on sedimentation rate but varies during the event (Hirschberg and Schubel 1979). However, because we are looking at the tracer profiles  $>20$  yr after the event, bioturbation probably has smeared this effect. Accordingly, we adopt the simplified assumption of Eq. 7.

For episodic erosion, a certain thickness of sediment is removed from the top of the sediment column at the time of the event. Excess  $^{210}\text{Pb}$  influx is assumed to equal  $F_0^{\text{pre}}[\text{Pb}]$  at all times and can be calculated from the following:

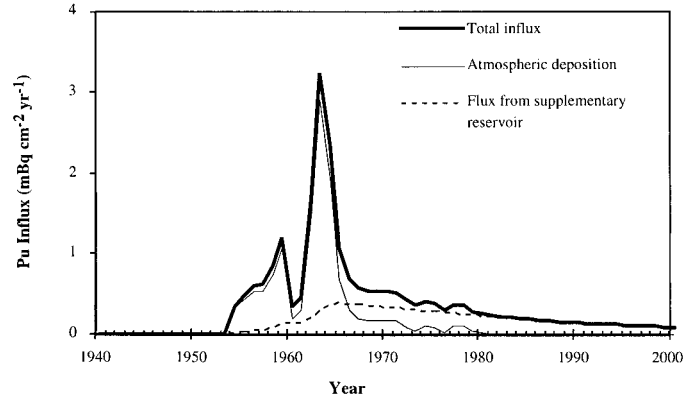


Fig. 2. History of Pu influx, under the assumption that total Pu in sediment is  $22 \text{ mBq cm}^{-2}$ , 59% Pu in sediment comes from direct atmospheric deposition ( $f = 0.59$ ), and the rest of Pu comes from the time-delayed reservoir. The residence time of Pu in the supplementary reservoir is 20 yr.

$$\begin{aligned} & \int_{t_0}^{t_c} F_0^{\text{pre}}[\text{Pb}] \times \exp[-\lambda(t_c - t)] dt \\ &= \rho \int_0^\infty C(1 - \phi) dx \\ &+ \rho \int_0^{x_{\text{event}}} C_{\text{event}}(1 - \phi) dx \exp[-\lambda(t_c - t_{\text{event}})], \quad (9) \end{aligned}$$

where  $x_{\text{event}}$  is the thickness of removed sediment and  $C_{\text{event}}$  is the activity of xs  $^{210}\text{Pb}$  in the sediment removed by erosion.

Atmospheric deposition of  $^{239,240}\text{Pu}$  varied with time because of historical changes in the number and magnitude of above-ground nuclear tests. The  $^{239,240}\text{Pu}$  fallout record was not measured directly but can be approximated as proportional to  $^{90}\text{Sr}$  deposition, because  $^{90}\text{Sr}$  is also a nuclear test product. Widespread atmospheric deposition of fissile material and fission products began in the early 1950s, increased steadily to 1963, and declined abruptly shortly after ratification of the Nuclear Test Ban Treaty (Fig. 2, thinner solid line). Our upper- and lower-Bay cores show buried  $^{239,240}\text{Pu}$  maxima (see below) that may plausibly be assigned to the maximum in fallout deposition in 1963. However, atmospheric deposition of weapons fallout had declined to very low values by the early 1970s (HASL 1977; Larsen 1985). Thus, the gradual decrease in  $^{239,240}\text{Pu}$  between the subsurface peak and the sediment surface in our upper-Bay core (see below) is incompatible with the history of fallout deposition. Moreover, our modeling shows that sediment mixing cannot explain this gradual decrease in  $^{239,240}\text{Pu}$ . To do so requires a second  $^{239,240}\text{Pu}$  input, supplied after most atmospheric deposition had ceased.

It is straightforward to simulate a supplementary  $^{239,240}\text{Pu}$  input by adding a time delay to atmospheric fallout deposition. Benninger and Dodge (1986) applied such a model to a record of  $^{239,240}\text{Pu}$  concentrations in annual bands of the coral *Montastrea annularis*. Robbins et al. (2000) developed an extension to the time-delay model, which they call the

“system time-average” approach. In both these instances, the time-averaged input was assumed to be the only source of  $^{239,240}\text{Pu}$  to the study site. Here, we treat the time-averaged  $^{239,240}\text{Pu}$  input as supplemental to the input from direct atmospheric deposition.

The influx of  $^{239,240}\text{Pu}$  from direct atmospheric deposition ( $F_{0(D)}^t[\text{Pu}]$ ) is assumed to be proportional to the flux of  $^{90}\text{Sr}$  fallout measured at New York City ( $F_{\text{Sr}}^t$ ):

$$F_{0(D)}^t[\text{Pu}] \propto F_{\text{Sr}}^t. \quad (10)$$

The proportionality in Eq. 10 is fixed by setting a value for  $f$  ( $0 \leq f \leq 1$ ), defined as the fraction of the total  $^{239,240}\text{Pu}$  inventory derived from direct atmospheric deposition, and imposing the following mass balance:

$$\int_{t_0}^{t_c} F_{0(D)}^t[\text{Pu}] dt = f\rho \int_0^\infty C(1 - \phi) dx. \quad (11)$$

Whenever there is finite  $^{239,240}\text{Pu}$  in the deepest sample, the profile is extrapolated to zero activity to evaluate the right-hand side of Eq. 11.

The supplemental input of  $^{239,240}\text{Pu}$  ( $F_{0(S)}^t[\text{Pu}]$ ) is treated as if derived from a reservoir which accumulated fallout Pu as it was deposited from the atmosphere and which continues to release it today. The  $^{239,240}\text{Pu}$  inventory in this reservoir at a certain time  $t$  is

$$\text{Inv}(t) \propto \int_{t_0}^t F_{\text{Sr}}^t \times \exp[-(t - t_0)/T] dt, \quad (12)$$

where  $T$  is the  $^{239,240}\text{Pu}$  residence time in the reservoir. The residence time cannot be identified with any single environmental reservoir, but the processes supplying the supplemental  $^{239,240}\text{Pu}$  might include erosion in the watershed and redistribution of sediment within the Bay. The flux of supplemental  $^{239,240}\text{Pu}$  from the “time-averaged” reservoir is proportional to the  $^{239,240}\text{Pu}$  inventory in the reservoir:

$$F_{0(S)}^t[\text{Pu}] \propto \text{Inv}(t), \quad (13)$$

with the proportionality fixed by the following mass balance:

$$\int_{t_0}^{t_c} F_{0(S)}^t[\text{Pu}] dt = (1 - f)\rho \int_0^\infty C(1 - \phi) dx. \quad (14)$$

Thus, the upper boundary condition for the steady-sedimentation  $^{239,240}\text{Pu}$  model is given by

$$F_0^t[\text{Pu}] = F_{0(D)}^t[\text{Pu}] + F_{0(S)}^t[\text{Pu}]. \quad (15)$$

The contribution of the supplementary reservoir with a residence time of 20 yr is illustrated in Fig. 2. Episodic deposition and erosion of  $^{239,240}\text{Pu}$  is simulated by an approach analogous to that used for  $x\text{s }^{210}\text{Pb}$  (Eqs. 7–9).

The lower-boundary conditions were set to be very deep (800 cm for  $x\text{s }^{210}\text{Pb}$  and 100 cm for  $^{239,240}\text{Pu}$ ), where we can safely assume that tracer activities are 0. Initial conditions for both  $x\text{s }^{210}\text{Pb}$  and  $^{239,240}\text{Pu}$  were set to zero (i.e., sediments are void of tracer at  $t = 0$ ). In the case of  $x\text{s }^{210}\text{Pb}$ , the simulation was begun in the year 1700 A.D. (i.e.,  $t_0 = 1,700$ ), to allow ample time to spin up to steady state. For  $^{239,240}\text{Pu}$ , the simulation was begun in the year 1950 (i.e.,  $t_0 = 1,950$ ),

well before the widespread release of fallout nuclides (Fig. 2).

Equation 1 is solved numerically (Sewell 2000), with boundary and initial conditions described above. The accuracy of the numerical solution is checked by comparing the total tracer influx with the sediment inventory calculated by integrating the predicted depth distributions. The difference between these two numbers is usually  $\leq 0.1\%$ .

Adjustable parameters in the model include: sedimentation rate ( $\omega_{\infty}^s$ ) before and after the event, mixing coefficient ( $D_{B_0}$ ), mixing depth parameter ( $x^*$ ), thickness of the storm deposition/erosion layer, transfer function parameters ( $P_{\text{Pb}}$  and  $P_{\text{Pu}}$  during and after the event), and, in the  $^{239,240}\text{Pu}$  case, fraction of sediment  $^{239,240}\text{Pu}$  from direct atmospheric deposition ( $f$ ) and residence time of  $^{239,240}\text{Pu}$  in the supplementary  $^{239,240}\text{Pu}$  reservoir ( $T$ ). We always start with the steady-state model. Our first guess of the mixed layer depth is from the thickness of the top sediment layer, which has nearly constant  $x\text{s }^{210}\text{Pb}$ , and the first guess of sedimentation rate is from the slope of  $\log(x\text{s }^{210}\text{Pb})$  versus depth evaluated below the apparent mixed layer.  $D_{B_0}$  is assumed to be  $5 \text{ cm}^2 \text{ yr}^{-1}$  at first. By comparing the model-generated  $x\text{s }^{210}\text{Pb}$  profile and the data, we can adjust the parameters to improve the fit to  $x\text{s }^{210}\text{Pb}$ . Using the parameters that yield a good fit for  $x\text{s }^{210}\text{Pb}$ , we then predict the  $^{239,240}\text{Pu}$  profile. By comparing the model-predicted  $^{239,240}\text{Pu}$  profile with the data, we adjust  $D_{B_0}$  and  $x^*$  to improve the fit for  $^{239,240}\text{Pu}$ . With each iteration, we check to ascertain that the adjusted parameters still generate a good fit for  $x\text{s }^{210}\text{Pb}$ . Our initial assumption is that the input history of  $^{239,240}\text{Pu}$  followed that of  $^{90}\text{Sr}$  at New York City (Eq. 10). When this input, as distributed by sediment accumulation and bioturbation, does not explain the shape of the  $^{239,240}\text{Pu}$  profile, the supplemental, time-averaged  $^{239,240}\text{Pu}$  input is added. In simulations, decreasing  $f$  (= fraction of sediment  $^{239,240}\text{Pu}$  from direct atmospheric deposition) results in higher  $^{239,240}\text{Pu}$  activity in the upper part of the sediment profile and a lower  $^{239,240}\text{Pu}$  peak activity (Fig. 2). Increasing the residence time ( $T$ ) of  $^{239,240}\text{Pu}$  in the supplementary reservoir causes simulated  $^{239,240}\text{Pu}$  to increase more gradually with depth below the sediment-water interface.

In general, the possible ranges of model parameters are small. Although many combinations of  $\omega_{\infty}^s$ ,  $D_{B_0}$ , and  $x^*$  might satisfactorily fit  $x\text{s }^{210}\text{Pb}$  alone, few yield good fits of both  $x\text{s }^{210}\text{Pb}$  and  $^{239,240}\text{Pu}$ . For example, a gradual decrease in  $x\text{s }^{210}\text{Pb}$  below the surficial, rapidly mixed layer might be ascribed to deep mixing rather than to sediment accumulation. Because deep mixing broadens the  $^{239,240}\text{Pu}$  peak, however, the  $^{239,240}\text{Pu}$  data limit the degree to which transport by sediment mixing can be substituted for transport by sediment accumulation. This is illustrated with the upper-Bay data (see below, in “Results and Discussion”).

We apply a nonsteady model only in those cases where the steady-state model cannot provide a satisfactory fit. If there is a change in slope in the  $x\text{s }^{210}\text{Pb}$  profile, the depth where the change occurs is assumed to be where the episodic event happened. Sedimentation rates calculated by linear regression of  $\log(x\text{s }^{210}\text{Pb})$  versus depth for different part of the profile are used as the first guess for pre- and post-event sedimentation rates. These values are varied systematically to get the best fit. If there is no obvious change in slope in

Table 1. Sampling sites and sediment properties for Chesapeake Bay.

Location	Upper-Bay	Mid-Bay	Lower-Bay
Station	ST2	ST5	ST7
Water depth (m)	6.5	21	15
$\phi_0$	0.90	0.97	0.70
$\phi_z$	0.81	0.78	0.57
$\beta$	0.13	0.09	0.44
LOI (wt.%)	9.5 $\pm$ 0.3	7.4 $\pm$ 1.5	2.8 $\pm$ 0.3
SiO <sub>2</sub> (wt.%)	53 $\pm$ 3	NA	73 $\pm$ 3
K ( $\mu$ mol g <sup>-1</sup> )	623 $\pm$ 17	NA	495 $\pm$ 23
Rel. inv.* xs <sup>210</sup> Pb	>2.8–3.7	0.9–1.2	1.7–2.2
Rel. inv.* <sup>239,240</sup> Pu	–2.2–2.4	0.18–0.19	0.59–0.64

$\phi_0$ ,  $\phi_z$ , and  $\beta$  are parameters in the exponential fit of porosity vs. depth (Eq. 2). NA = data not available.

\* Rel. inv. (i.e., relative inventory) = (sediment inventory)/(inventory supported by direct atmospheric deposition). Relative inventories of all nuclides at the upper-Bay site are underestimated because the deepest samples contain finite activity. Direct atmospheric deposition: xs<sup>210</sup>Pb = 327–427 mBq cm<sup>-2</sup> (Graustein and Turekian 1986); <sup>239,240</sup>Pu = 8.9–9.6 mBq cm<sup>-2</sup> (Hardy et al. 1973). Sediment inventories are decay-corrected to the time of sampling (30 June–1 July 1994).

the xs <sup>210</sup>Pb profile, we still begin with a sedimentation rate determined by the slope of log(xs <sup>210</sup>Pb) versus depth. In such cases, we would ideally find literature reports of potentially significant events in the sedimentary environment. Lacking such reports, it may still be instructive to experiment with possible events. Thickness of a storm deposition/erosion layer is based on the thickness of an anomalous layer in profiles of lithologic properties (e.g., K, LOI, porosity). Transfer function parameters during the episodic event determine the degree of offset in tracer profiles within the storm layer.

Data features used for selecting good fit include (1) fit of the general shape of the profiles judged subjectively, (2) fit of the prominent features in the tracer profiles, (3) gradient of xs <sup>210</sup>Pb profile below the mixed layer, (4) depth and shape of the <sup>239,240</sup>Pu peak, and (5) penetration depth of <sup>239,240</sup>Pu. In our best-constrained example (upper Bay), we found that fitting both xs <sup>210</sup>Pb and <sup>239,240</sup>Pu profiles restricted all parameters to lie within narrow ranges.

## Results and discussion

**Sediment lithology**—Variations in bulk sediment properties (porosity, LOI) and major element (SiO<sub>2</sub>, K) concentrations serve as indicators of changes in sediment lithology. In general, these parameters vary far more dramatically among our 3 sites than within cores. Therefore, only average values are given in Table 1. For porosity, the parameters of exponential fit for porosity profiles are given (i.e.,  $\phi_0$ ,  $\phi_z$ , and  $\beta$ ; Eq. 2). Porosity and LOI are much lower in the lower-Bay core, suggesting coarser grain size and reduced organic content. Higher SiO<sub>2</sub> in the lower-Bay core (73%  $\pm$  3%, compared with 53%  $\pm$  3% in the upper-Bay) probably reflects a greater abundance of quartz. Coarse grain size and elevated quartz content at the lower-Bay site dilute elements and tracers that associate with fine particles and organic mat-

ter. Where appropriate, we use within-core indicators of lithologic change to refine sediment chronology (see below).

**Sediment inventories of particle-reactive radionuclides**—Inventories of radionuclides provide a convenient means of evaluating sediment focusing or comparing efficiencies of particle scavenging. Relative inventories of xs <sup>210</sup>Pb and <sup>239,240</sup>Pu are calculated by summing the product of activities (mBq g<sup>-1</sup>) and mass depth (g cm<sup>-2</sup>) and dividing by the inventories supported by direct atmospheric deposition. Rapid and quantitative scavenging of atmosphere-derived radionuclides onto particles, followed by permanent transfer of only these particles to the sediment below, would result in a relative inventory equal to one. In contrast, sediment focusing and differences in particle scavenging may cause a relative inventory different from 1 (Benninger et al. 1979; Appleby and Oldfield 1992).

<sup>210</sup>Pb is strongly particle-reactive in estuaries (e.g., Benninger 1979; Santschi et al. 1979). The sediment inventory of xs <sup>210</sup>Pb at the mid-Bay site is essentially the same as direct atmospheric deposition (Table 1). However, at lower- and upper-Bay sites, sediment inventories exceed atmospheric deposition by factors of  $\sim$ 2 and 3, respectively. This suggests that these two sites serve as depocenters for particles and/or efficiently scavenge <sup>210</sup>Pb.

Fallout <sup>239,240</sup>Pu shows the same pattern in the distribution of sediment inventories (upper-Bay > lower-Bay > mid-Bay). With <sup>239,240</sup>Pu, however, only the upper-Bay core contains an inventory exceeding direct atmospheric deposition; mid-Bay (0.2 $\times$  atmospheric deposition) and lower-Bay (0.6 $\times$ ) sediment accumulated <sup>239,240</sup>Pu much less efficiently than xs <sup>210</sup>Pb (Table 1). Even the upper-Bay core has a relatively low relative inventory of <sup>239,240</sup>Pu compared with xs <sup>210</sup>Pb (2 $\times$  atmospheric deposition, as opposed to 3 $\times$ ). In contrast to the approximately steady-state atmospheric deposition of xs <sup>210</sup>Pb (Appleby and Oldfield 1978), most of the flux of fallout <sup>239,240</sup>Pu occurred between 1955 and 1965 (HASL 1977; Larsen 1985). Thus, lower <sup>239,240</sup>Pu inventories relative to xs <sup>210</sup>Pb could reflect greater dilution of <sup>239,240</sup>Pu-tagged particles with sediments either too “old” or too “young” to have acquired significant <sup>239,240</sup>Pu. It is also possible that <sup>239,240</sup>Pu was less efficiently scavenged from Bay waters than was <sup>210</sup>Pb. If this is the case, <sup>239,240</sup>Pu scavenging is markedly less efficient in the mid- and lower Bay, compared with the upper Bay.

**Sediment chronology**—Sedimentation and mixing rates in the Chesapeake Bay and its subestuaries have been reported in many studies (e.g., Goldberg et al. 1978; Hirschberg and Schubel 1979; Officer et al. 1984; Helz et al. 1985/1986; Dibb and Rice 1989; Donoghue 1990; Cooper and Brush 1991; McLean et al. 1991; Cornwell et al. 1996; Zimmerman and Canuel 2000). However, these rates are inferred from depth profiles of a single tracer and do not differentiate between normal sedimentation and episodic deposition or erosion. The most complete study of recent sedimentation in Chesapeake Bay is presented in Officer et al. (1984). They reanalyzed existing xs <sup>210</sup>Pb, <sup>137</sup>Cs, and <sup>239,240</sup>Pu data from throughout the Bay using a model that assumes constant sedimentation and simulates bioturbation as diffusive mixing in

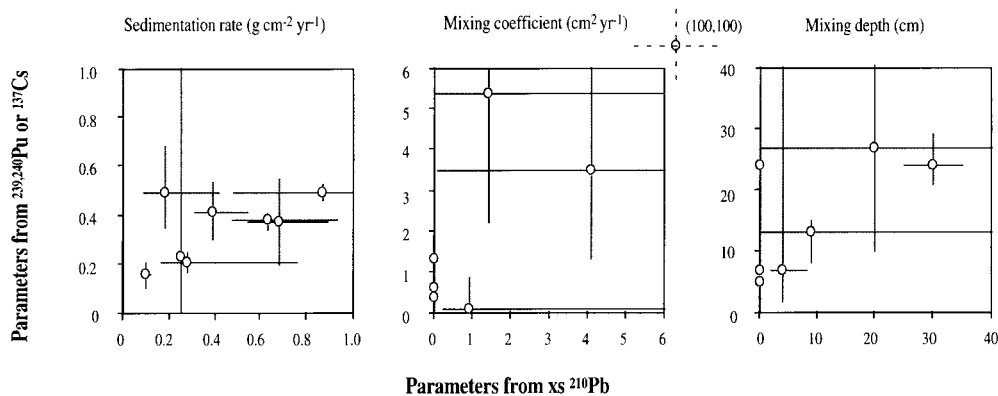


Fig. 3. Comparison of sedimentation rates, mixing coefficients and mixing depths for Chesapeake Bay sediments predicted by curve fitting to either  $x_s$   $^{210}\text{Pb}$  or fallout nuclides ( $^{137}\text{Cs}$  or  $^{239,240}\text{Pu}$ ) profiles. Error bars indicate uncertainty in the model-derived parameter (95% confidence intervals). Data are from Officer et al. (1984).

a surface layer of finite thickness. Their results show that optimum values of sedimentation rate, mixing coefficient, and mixing depth predicted by curve-fitting to a single tracer are generally different for  $x_s$   $^{210}\text{Pb}$  and fallout isotopes (Fig. 3). The large confidence intervals on parameters estimated from a single tracer permitted the hypothesis that results from  $x_s$   $^{210}\text{Pb}$  and fallout nuclides were in substantial agreement. In this study, we use the same sediment transport parameters for  $x_s$   $^{210}\text{Pb}$  and  $^{239,240}\text{Pu}$ . Our optimum parameters for fitting both  $x_s$   $^{210}\text{Pb}$  and  $^{239,240}\text{Pu}$  profiles are listed in Table 2.

*Upper-Bay*—The  $x_s$   $^{210}\text{Pb}$  profile from the upper-Bay is somewhat erratic in the upper 10 cm, then shows a smooth decline to a depth of  $\sim 30$  cm (Fig. 4A). Excess  $^{210}\text{Pb}$  activity increases abruptly in the depth interval just below 30 cm but then decreases gradually through the remainder of the core. Total  $^{210}\text{Pb}$  in the deepest sample exceeds supported levels by nearly a factor of 2.

The  $^{239,240}\text{Pu}$  profile shows a broad, well-defined subsurface peak at  $\sim 42$  cm (Fig. 4B). Activities of  $^{239,240}\text{Pu}$  are finite throughout the core, even at the sediment-water interface. The core did not penetrate to depths containing sediment free of fallout nuclides.

Results of our initial  $x_s$   $^{210}\text{Pb}$  and  $^{239,240}\text{Pu}$  simulations assuming steady-state sedimentation are shown as solid curves in Fig. 4A,B. Fits to both tracers were generated with  $\omega_z = 1.05$   $\text{cm yr}^{-1}$  ( $0.48$   $\text{g cm}^{-2} \text{yr}^{-1}$ ),  $D_{B_0} = 10$   $\text{cm}^2 \text{yr}^{-1}$ , mixed layer depth = 10 cm,  $f = 0.65$ , and  $T = 40$  yr. To illustrate the advantage of two-tracer approach, we also show a model result that can simulate the  $x_s$   $^{210}\text{Pb}$  profile reasonably well by deeper mixing and a slower sedimentation rate ( $\omega_z = 0.8$   $\text{cm yr}^{-1}$ ,  $D_{B_0} = 3$   $\text{cm}^2 \text{yr}^{-1}$ , mixed layer depth = 27 cm,  $f = 0.65$ , and  $T = 40$  yr) but does a poor job simulating the  $^{239,240}\text{Pu}$  profile (Fig. 4A,B, dashed lines).

Although the steady sedimentation model can do a reasonable job of simulating both tracer profiles, the model systematically underestimates  $x_s$   $^{210}\text{Pb}$  activities in the 7–12-cm depth interval and overestimates values between 20 and 30 cm. Furthermore, the model fails to account for several pronounced features in the tracer profiles. For example, the

model-derived  $x_s$   $^{210}\text{Pb}$  curve does not reproduce the discontinuity at  $\sim 30$  cm (Fig. 4A). Likewise, the predicted  $^{239,240}\text{Pu}$  profile blurs the sharp increase in activity immediately below 30 cm (Fig. 4B).

Excess  $^{210}\text{Pb}$  is not the only profile from the upper-Bay site with an anomalous “break” at a depth of 30 cm. Discontinuities in porosity,  $K$ , and  $^{137}\text{Cs}/^{239,240}\text{Pu}$  ratio at depths of  $\sim 30$  cm (Fig. 4G–I) suggest an abrupt change in sediment lithology and/or sources. The consistency of these features suggests that discrepancies between the constant sedimentation model and data may be related to a major storm event rather than random noise in the  $x_s$   $^{210}\text{Pb}$  and  $^{239,240}\text{Pu}$  data. Using the steady-state model as a guide, we predict that anomalous sedimentation occurred some time in the early 1970s.

Tropical storm Agnes blew over Chesapeake Bay in late June and early July 1972, causing record or near-record historical floods in the major tributaries (Schubel 1977; USGS Water Data, Susquehanna River at Harrisburg, PA, 1891–1998; <http://waterdata.usgs.gov/nwis-w/US/>). A number of studies provide evidence that the storm caused rapid sediment deposition in some regions of the upper Bay. Gross et al. (1978) estimate that the flood caused by Agnes transported in a 2-week period an amount of sediment equivalent to  $>30$  yr of normal sediment transport. During the peak flood period, suspended sediment loads from the Susquehanna River were 31–62 times higher than normal (Schubel 1977). However, the flux of suspended sediment to the middle and lower reaches of the Bay was only 2–3 times higher than normal (Schubel 1977). This suggests that most of the excess sediment loading was trapped within the upper Bay. Helz et al. (1985/86) attribute a 5–10-cm-thick layer of sediment with uniform  $x_s$   $^{210}\text{Pb}$  activity in their upper-Bay cores to rapid deposition associated with the passage of Agnes.

We used our nonsteady model to test the hypothesis that  $x_s$   $^{210}\text{Pb}$  and  $^{239,240}\text{Pu}$  profiles from our upper-Bay site have been affected by episodic deposition during the Agnes flood. Under the assumption of constant sedimentation before and after the event, fits to both tracers were generated with  $\omega_z = 0.98$   $\text{cm yr}^{-1}$  ( $0.45$   $\text{g cm}^{-2} \text{yr}^{-1}$ ),  $D_{B_0} = 10$   $\text{cm}^2 \text{yr}^{-1}$ , mixed layer depth = 9 cm,  $P_{\text{pb}}^{\text{event}} = 0.5$ ,  $P_{\text{pu}}^{\text{event}} = 0.6$ ,  $f = 0.59$ ,  $T$

Table 2. Sediment transport parameters generating fits for both  $x_s^{210}\text{Pb}$  and  $^{239,240}\text{Pu}$ .

Location	Upper-Bay	Mid-Bay	Lower-Bay	
Station	ST2	ST5	ST7	
Scenario	Episodic deposition	Constant $\omega$	Decreased $\omega$	Episodic erosion
$\omega_z^{\text{pre}}$ (cm yr <sup>-1</sup> )	1.3	≤0.05	1.2	0.7
$\omega_z^{\text{post}}$ (cm yr <sup>-1</sup> )	0.87	—	0.4	0.75
$F_{\text{SM}}^{\text{pre}}$ (g cm <sup>-2</sup> yr <sup>-1</sup> )	0.60	≤0.028	1.3	0.7
$F_{\text{SM}}^{\text{post}}$ (g cm <sup>-2</sup> yr <sup>-1</sup> )	0.40	—	0.4	0.75
$x_{\text{event}}$ (cm)*	5 (deposition)	—	0	10 (erosion)
$t_{\text{event}}$ (A.D.)†	1972	—	1965	1994
$P_{\text{Pb}}^{\text{event}}$	0.45	—	—	—
$P_{\text{Pu}}^{\text{event}}$	0.75	—	—	—
$P_{\text{Pb}}^{\text{post}}$	0.1	—	1	—
$P_{\text{Pu}}^{\text{post}}$	0.4	—	1	—
$f$	0.59	1	0.5	0.6
$T$ (yr)	20	—	60	20
$D_{B_0}$ (cm <sup>2</sup> yr <sup>-1</sup> )	10	25–40	1	50, 1‡
Mixed layer depth (cm)	9	7–10	32	3, 32‡

\*  $x_{\text{event}}$  is the thickness of the storm sediment during episodic deposition or the thickness of the removed sediment during episodic sediment erosion.

†  $t_{\text{event}}$  is the time of the episodic event.

‡ Two-layer mixing; see details in text.

= 20 yr, and a storm layer thickness of 5 cm. As shown in Fig. 4C,D, the model yields good fits for both tracers. The model-derived  $x_s^{210}\text{Pb}$  curve simulates the sudden increase in activity below 30 cm (Fig. 4C), whereas the model-derived  $^{239,240}\text{Pu}$  profile provides a nearly perfect fit to the data (Fig. 4D). Furthermore, the thickness of the storm layer predicted by the model (5 cm) is consistent with the 5–10-cm layer with constant  $x_s^{210}\text{Pb}$  observed by Helz et al. (1985/1986). However, the depth of the Agnes layer predicted by the simulation (28–33 cm) is not consistent with anomalies in profiles of porosity, K, and  $^{137}\text{Cs}/^{239,240}\text{Pu}$  ratio, which suggest that the region between 25–30 cm is a more probable zone for a layer of storm-derived sediment. Reduced porosity in this interval (Fig. 4G) is consistent with delivery of coarser particles during the period of high flow. Anomalous K concentrations (Fig. 4H) are not surprising, given that sediments remobilized from river banks and terrestrial sources may have a distinct lithology. Elevated values of  $^{137}\text{Cs}/^{239,240}\text{Pu}$  ratio (Fig. 4I) are consistent with the expectation that the Agnes layer is enriched in terrestrial sediment ( $^{137}\text{Cs}/^{239,240}\text{Pu}$  ratios are lower in marine-derived particles because of inefficient fixation of  $^{137}\text{Cs}$  in brackish waters).

Differences in depth between the model-derived storm layer and anomalies in sediment profiles can be reconciled by allowing for slower sedimentation after the passage of tropical storm Agnes. There is evidence that flooding from Agnes could have affected sedimentation long after passage of the storm. A core collected from the Conowingo reservoir of the Susquehanna River exhibited a distinct break in the  $x_s^{210}\text{Pb}$  profile, which Helz et al. (1985/1986) attribute to an erosion event. Their calculations suggest that the erosion occurred between 1970 and 1972, consistent with Agnes; the thickness of the missing section was estimated to be ~70 cm. Removal of large amounts of sediment from major sources in the Susquehanna River valley could result in a long-term reduction in sediment delivery to the upper-Bay (Meade 1982).

Allowing for a decreased sedimentation rate after the passage of Agnes, we get fits to both tracers with  $\omega_z^{\text{pre}} = 1.3$  cm yr<sup>-1</sup> (0.60 g cm<sup>-2</sup> yr<sup>-1</sup>),  $\omega_z^{\text{post}} = 0.87$  cm yr<sup>-1</sup> (0.40 g cm<sup>-2</sup> yr<sup>-1</sup>),  $D_{B_0} = 10$  cm<sup>2</sup> yr<sup>-1</sup>, mixed layer depth = 9 cm,  $P_{\text{Pb}}^{\text{event}} = 0.45$ ,  $P_{\text{Pu}}^{\text{event}} = 0.75$ ,  $P_{\text{Pb}}^{\text{post}} = 0.1$ ,  $P_{\text{Pu}}^{\text{post}} = 0.4$ ,  $f = 0.59$ ,  $T = 20$  yr, and a storm layer thickness of 5 cm (Table 2). Accounting for reduced sediment supply after Agnes predicts a storm layer at 25–30 cm (Fig. 4E,F), consistent with anomalies in porosity, K, and  $^{137}\text{Cs}/^{239,240}\text{Pu}$  profiles (Fig. 4G–I).

Finite  $^{239,240}\text{Pu}$  in the upper 20 cm requires that ~40% of the tracer influx is derived from the “time-averaged” reservoir (i.e.,  $f = 0.59$ ). This relatively large supplementary input is consistent with a sediment  $^{239,240}\text{Pu}$  inventory at the upper-Bay station that exceeds direct atmospheric deposition by a factor of ~2 (Table 1). A 20-yr residence time for the “time-averaged” reservoir yields a fit to the data. Although longer residence times ( $T > 100$  yr) cannot be ruled out, a value of ~20 yr is necessary to accurately reproduce the consistent decrease in  $^{239,240}\text{Pu}$  at depths above 20 cm (Fig. 4F). Our estimated residence time for the “time-averaged” reservoir is consistent with values reported for  $^{239,240}\text{Pu}$  influx at other shallow-water, near-shore environments (e.g., 10–50 yr for Lake Michigan, Robbins et al. 1998; 15–20 yr for Florida Bay, Robbins et al. 2000).

The transfer function parameter for  $^{210}\text{Pb}$  during the event ( $P_{\text{Pb}}^{\text{event}} = 0.45$ ) implies that the influx of  $x_s^{210}\text{Pb}$  increased during the period of episodic deposition but did not keep pace with the increase in bulk sedimentation rate. As a result, sediments deposited during the storm had reduced activity of  $x_s^{210}\text{Pb}$ . Helz et al. (1985/1986) also note lower  $x_s^{210}\text{Pb}$  activity in the storm layer associated with Agnes. Using their profiles and assuming a normal sedimentation rate of 1 cm yr<sup>-1</sup> interrupted by rapid deposition over a 2-week period, we calculate  $P_{\text{Pb}}^{\text{event}}$  values ranging from 0.3 to 0.7, consistent with our model predictions. The predicted transfer function parameter for  $^{239,240}\text{Pu}$  during the event ( $P_{\text{Pu}}^{\text{event}} = 0.75$ ) implies

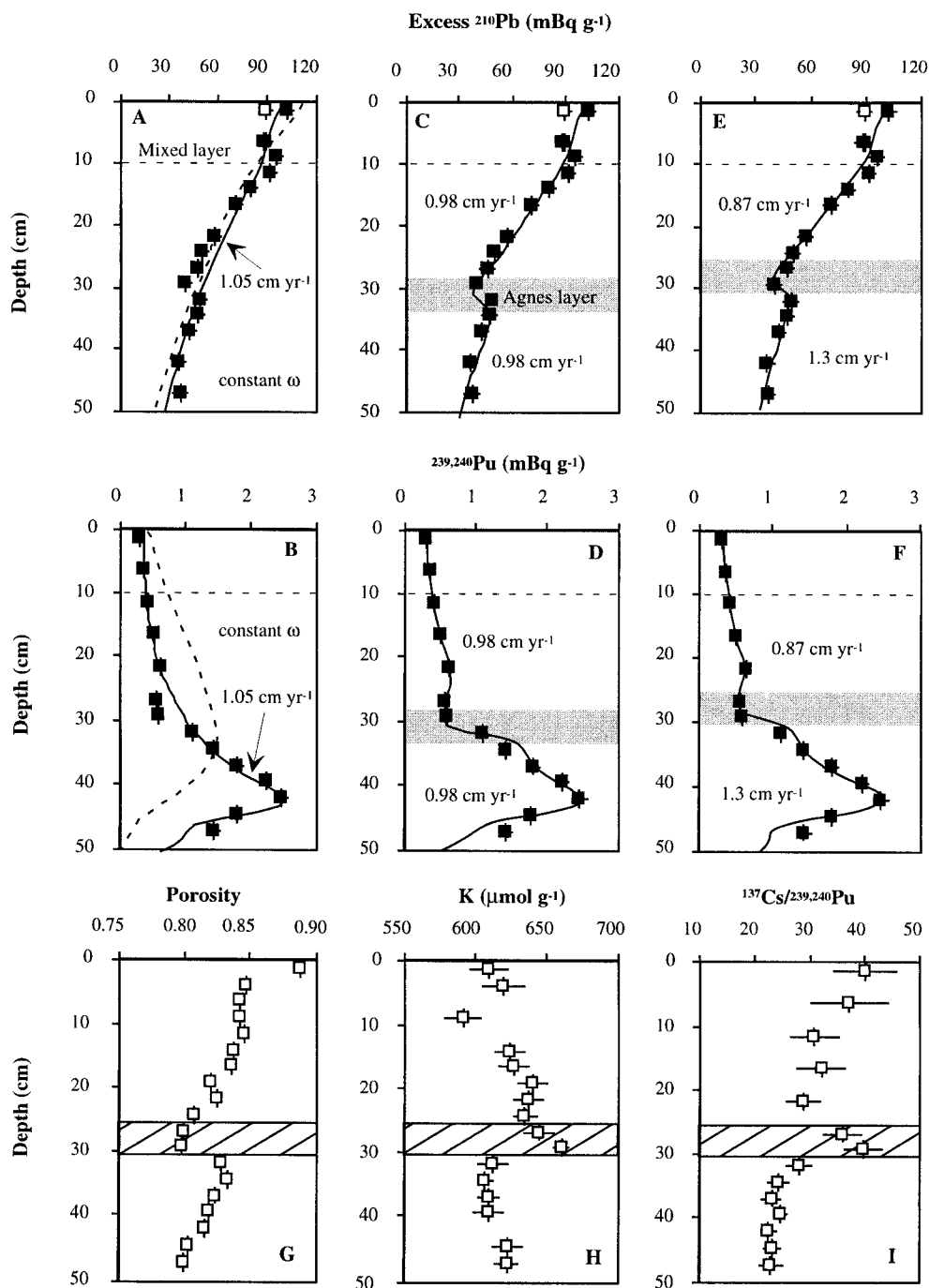


Fig. 4. Excess  $^{210}\text{Pb}$ ,  $^{239,240}\text{Pu}$ , porosity, K, and  $^{137}\text{Cs}/^{239,240}\text{Pu}$  versus sediment depth at the upper-Bay site. The horizontal band at  $\sim 30$  cm is the storm deposit from tropical storm Agnes. The solid and dashed curves in xs  $^{210}\text{Pb}$  and  $^{239,240}\text{Pu}$  profiles are the results of modeling. (A and B) Steady-state accumulation: solid curves are fits for both tracers, and dashed curves are results of slower sedimentation rate and deeper mixing, which generate a good fit for xs  $^{210}\text{Pb}$  but a poor fit for  $^{239,240}\text{Pu}$ . (C and D) 5-cm storm deposition with the same sedimentation rate before and after the episodic event. (E and F) 5-cm storm deposition and reduced sedimentation rate after the passage of Agnes (see text). Empty and solid squares are xs  $^{210}\text{Pb}$  activities before and after correcting for Rn loss, respectively. Horizontal error bars denote  $\pm 1$  SD; absence of an error bar indicates that uncertainty is less than symbol size. Vertical error bars indicate the sampling interval. Horizontal dashed lines indicate the mixed layer depth. Filled bands indicate the storm layer predicted by the model, and hatched bands represent the anomalous layer indicated by (G) porosity, (H) K, and (I)  $^{137}\text{Cs}/^{239,240}\text{Pu}$ .

an increase in influx and decrease in activity during the period of rapid deposition. Both during the event and after the event, transfer function parameters for  $^{239,240}\text{Pu}$  are higher than those for  $x_s$   $^{210}\text{Pb}$ , suggesting that  $^{239,240}\text{Pu}$  influx is less affected by changes in sedimentation rate. This pattern is consistent with the fact that the relative inventory of  $^{239,240}\text{Pu}$  ( $>2.2$ – $2.4$ ) is lower than that of  $x_s$   $^{210}\text{Pb}$  ( $>2.8$ – $3.7$ ), and therefore a larger fraction of  $x_s$   $^{210}\text{Pb}$  in the sediment comes from sources other than direct atmospheric deposition.

The composition of the Agnes sediment might be different from the normal deposition sequence because the extreme discharge tapped floodplain sediment sources that are not mobilized by more typical peak discharges. Schubel and Zabawa (1977) found no significant difference in sediment size or mineralogy between Agnes and pre-Agnes sediments in their cores. However, they reported “extreme lateral variability” of internal sedimentary structures over short distances, so that deposition may have been very patchy. Our proposed event sediment had lower  $x_s$   $^{210}\text{Pb}$  and porosity, and higher K and  $^{137}\text{Cs}/^{239,240}\text{Pu}$ , than pre-Agnes sediment (Fig. 4). Moreover, we can detect these contrasts despite bioturbation in the years after Agnes. Thus, we suggest that sediment lithology in, and/or sediment sources to, the Agnes layer in our upper-Bay core probably differed from previous deposition at this site.

**Mid-Bay**—Excess  $^{210}\text{Pb}$  in the upper 10 cm of the mid-Bay core displays uniform activity, which drops rapidly to 0 at  $\sim 15$  cm depth (Fig. 5A).  $^{239,240}\text{Pu}$  activities are also nearly constant in the upper 10 cm and decrease rapidly to 0 in concert with  $x_s$   $^{210}\text{Pb}$  (Fig. 5B). The similarity of  $x_s$   $^{210}\text{Pb}$  and  $^{239,240}\text{Pu}$  profiles suggests that both tracers are influenced largely by sediment mixing. Excess  $^{210}\text{Pb}$  in the upper section is higher than we observe in the upper Bay. This implies that the particles deposited here had very high initial concentrations of  $x_s$   $^{210}\text{Pb}$ .

Following our modeling strategy, we first simulated the mid-Bay data with a steady-state model. When mixing dominates over advection, modeling provides only an upper limit for the sediment accumulation rate. Thus, sediment profiles of  $x_s$   $^{210}\text{Pb}$  and  $^{239,240}\text{Pu}$  can be simulated with a maximum  $\omega_z = 0.05$   $\text{cm yr}^{-1}$  ( $0.028$   $\text{g cm}^{-2} \text{yr}^{-1}$ ),  $D_{B_0} = 40$   $\text{cm}^2 \text{yr}^{-1}$ , and mixed layer depth = 7 cm (Fig. 5A,B; Table 2). A higher sedimentation rate cannot simulate the steep  $x_s$   $^{210}\text{Pb}$  change below the mixed layer. Although a higher sedimentation rate can be ruled out, any  $\omega_z$  value  $\leq 0.05$   $\text{cm yr}^{-1}$  can reproduce the observed  $x_s$   $^{210}\text{Pb}$  and  $^{239,240}\text{Pu}$  profiles. For example, assuming zero sedimentation with  $D_{B_0} = 25$   $\text{cm}^2 \text{yr}^{-1}$ , and mixed layer depth = 10 cm provides a comparable fit to the data (not shown). Model results are not sensitive to the values of  $f$  and  $T$  ( $f = 1$  is assumed for the simulation).

The maximum sedimentation rate predicted by the steady-state model confirms that sediment mixing dominates over advection. Because  $^{239,240}\text{Pu}$  was introduced into the environment no earlier than 1945, the upper-limit sedimentation rate ( $\omega_z \leq 0.05$   $\text{cm yr}^{-1}$ ) suggests a maximum penetration depth of 2.5 cm in the absence of mixing. Thus, mixing is likely to be the major mechanism for moving the  $^{239,240}\text{Pu}$  to depths  $>10$  cm.

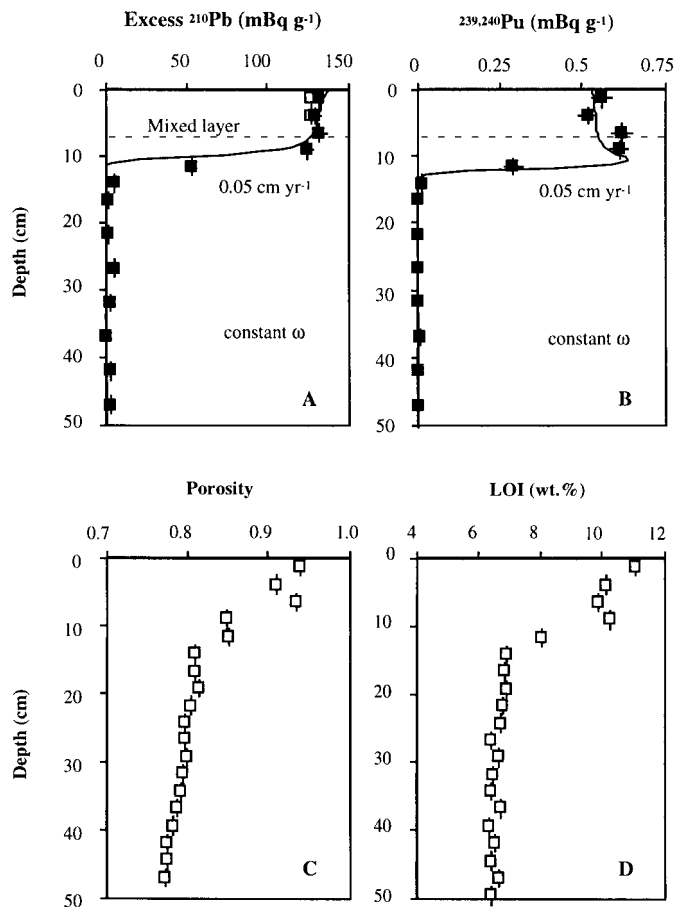


Fig. 5. Excess  $^{210}\text{Pb}$ ,  $^{239,240}\text{Pu}$ , porosity, and LOI versus sediment depth at the mid-Bay site. The solid curves in  $x_s$   $^{210}\text{Pb}$  and  $^{239,240}\text{Pu}$  profiles are the results of modeling. Empty and solid squares are  $x_s$   $^{210}\text{Pb}$  activities before and after correcting for Rn loss, respectively. Horizontal error bars denote  $\pm 1$  SD; absence of an error bar indicates that uncertainty is less than symbol size. Vertical error bars indicate the sampling interval. Horizontal dashed lines indicate the mixed layer depth.

It is apparent that nonsteady processes might equally well have generated the mid-Bay profiles of  $x_s$   $^{210}\text{Pb}$  and  $^{239,240}\text{Pu}$ . As noted, core-top  $x_s$   $^{210}\text{Pb}$  is substantially higher at the mid-Bay site than elsewhere. In addition, the ratio of the relative inventories,  $x_s$   $^{210}\text{Pb}/^{239,240}\text{Pu}$  (Table 1), is highest at the mid-Bay site. These observations might be explained, for example, by recent, rapid deposition of the surface layer (less than  $\sim 10$  cm), followed by limited mixing with the more consolidated sediment below  $\sim 10$  cm (Fig. 5). In this scenario, intervals of erosion or nondeposition might alternate with intervals of rapid sediment deposition. Averaged over the useful range of  $x_s$   $^{210}\text{Pb}$  ( $\sim 100$  yr), the net sedimentation rate would still be low.

A low net sedimentation rate at the mid-Bay site is consistent with published results. Officer et al. (1984) suggested that the mid-Bay is the seaward limit of deposition of sediment discharged from the Susquehanna River and the landward limit for sediment derived from the continental shelf. Thus sediment supply might limit the sedimentation rate.

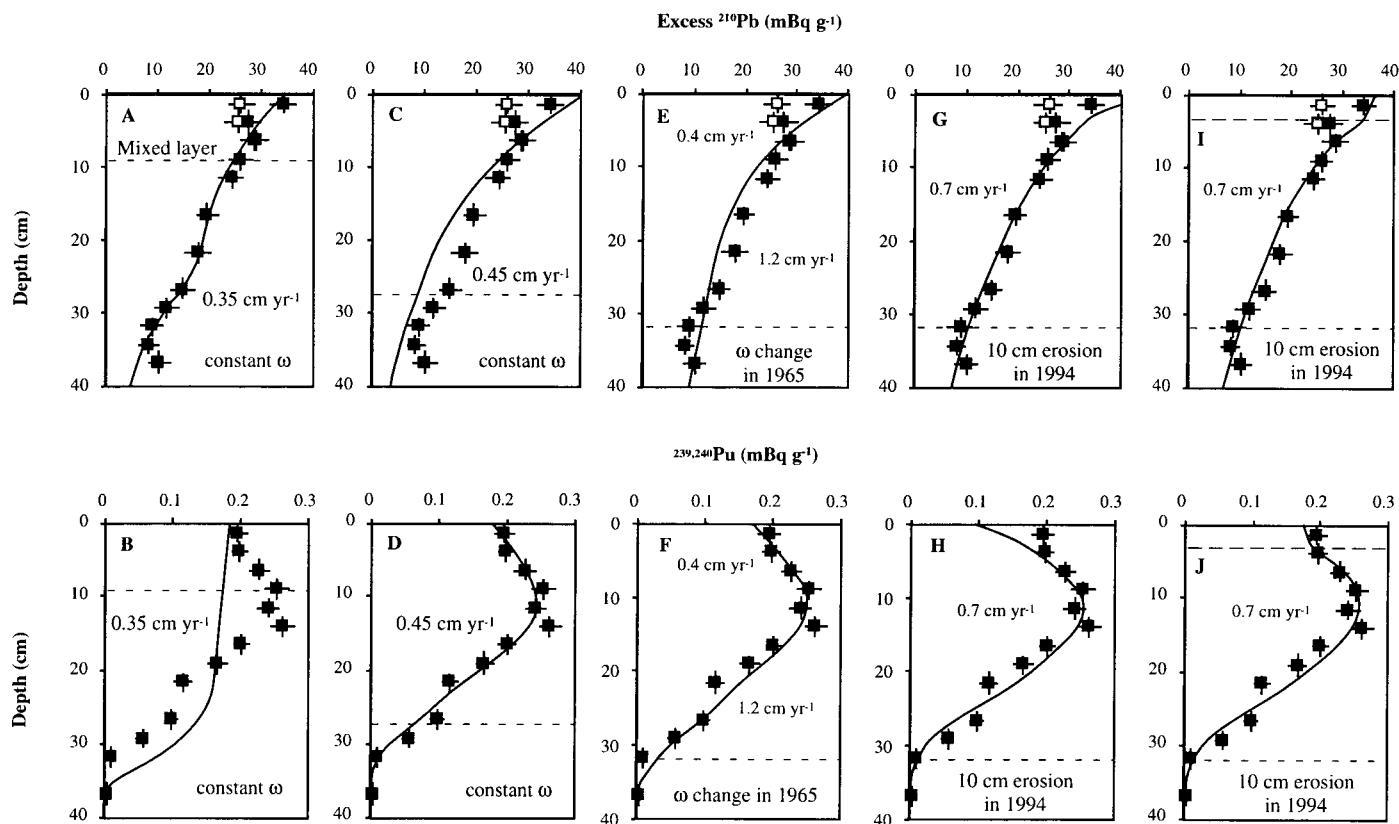


Fig. 6. Excess  $^{210}\text{Pb}$  and  $^{239,240}\text{Pu}$  versus sediment depth at the lower-Bay site. (A and B) Modeling results under the assumption of steady-state accumulation that fit  $x_s$   $^{210}\text{Pb}$  profile yet do not fit  $^{239,240}\text{Pu}$  profile. (C and D) Modeling results under the assumption of steady-state accumulation that fit  $^{239,240}\text{Pu}$  profile but do not fit  $x_s$   $^{210}\text{Pb}$  profile. (E and F) Modeling results under the assumption of sedimentation rate changes from 1.2 to 0.4  $\text{cm yr}^{-1}$  in 1965. (G and H) Modeling results under the assumption of erosional sediment loss of 10 cm in 1994 with one-layer mixing. (I and J) Modeling results under the assumption of erosional sediment loss of 10 cm in 1994 with two-layer mixing (see text). Empty and solid squares are  $x_s$   $^{210}\text{Pb}$  activities before and after correcting for Rn loss, respectively. Horizontal error bars denote  $\pm 1$  SD; absence of an error bar indicates that uncertainty is less than symbol size. Vertical error bars indicate the sampling interval. Horizontal dashed lines indicate the mixed layer depth. In (I) and (J), horizontal dashed lines at 3 and 32 cm depth indicate the depth of rapidly mixed layer and slowly mixed layer, respectively.

Additionally, Schubel and Carter (1977) have argued that the major tributary estuaries of Chesapeake Bay are sinks for Bay suspended sediment; our mid-Bay site is opposite of mouth of one of these estuaries (Patuxent River).

**Lower Bay**—Profiles of  $x_s$   $^{210}\text{Pb}$  and  $^{239,240}\text{Pu}$  in the lower-Bay core appear deceptively simple:  $x_s$   $^{210}\text{Pb}$  generally decreases downcore (Fig. 6A) and  $^{239,240}\text{Pu}$  shows a broad but recognizable peak at 10–15 cm (Fig. 6B). However, the sediment chronology at this site is complex and serves to illustrate the utility of coupling  $x_s$   $^{210}\text{Pb}$  and fallout nuclides to constrain sedimentation rates.

Our initial simulation, which assumes a constant sedimentation rate, did an excellent job of reproducing the  $x_s$   $^{210}\text{Pb}$  profile (Fig. 6A) with  $\omega_z = 0.35$   $\text{cm yr}^{-1}$ ,  $D_{B_0} = 9$   $\text{cm}^2 \text{yr}^{-1}$ , and mixed layer depth = 24 cm. However, these sedimentation and mixing rates predict a  $^{239,240}\text{Pu}$  profile that is inconsistent with the data (Fig. 6B). The steady-sedimentation model could be tuned to accurately simulate the  $^{239,240}\text{Pu}$  data (Fig. 6D) with  $\omega_z = 0.45$   $\text{cm yr}^{-1}$ ,  $D_{B_0} = 1$   $\text{cm}^2 \text{yr}^{-1}$ , mixed layer depth = 27 cm,  $f = 0.4$ ,  $T = 60$  yr; but for

these values the  $x_s$   $^{210}\text{Pb}$  profile is poorly predicted (Fig. 6C). The inability of the steady-sedimentation model to simulate both tracer profiles with a single set of  $\omega_z$ ,  $D_{B_0}$ , and  $x^*$  values suggests that episodic events may have influenced tracer distributions in sediments from this site.

We used our nonsteady model to test three possible scenarios: (1) a sudden change in sedimentation rate, (2) an erosion event, and (3) a depositional event. A dramatic decrease in sedimentation rate after 1965 (1.2 to 0.4  $\text{cm yr}^{-1}$ ) with  $D_{B_0} = 1$   $\text{cm}^2 \text{yr}^{-1}$ , mixed layer depth = 32 cm,  $f = 0.5$ , and  $T = 60$  yr (Table 2) yields reasonable fits for  $x_s$   $^{210}\text{Pb}$  (Fig. 6E) and  $^{239,240}\text{Pu}$  (Fig. 6F). Although consistency between simulated and measured profiles suggests that this scenario is plausible, we are unable to find any evidence in the literature to support or explain such a large change in the sedimentation rate.

Sedimentation and mixing rates from  $x_s$   $^{210}\text{Pb}$  and  $^{239,240}\text{Pu}$  profiles can also be reconciled if sediment from this site experienced significant erosion within 2 yr of the time that cores were collected. Under the assumption that an event in 1994 eroded 10 cm of sediment, we get reasonable fits for

xs  $^{210}\text{Pb}$  (Fig. 6G) and  $^{239,240}\text{Pu}$  (Fig. 6H) with  $\omega_{\infty} = 0.7 \text{ cm yr}^{-1}$  ( $0.75 \text{ g cm}^{-2} \text{ yr}^{-1}$ ),  $D_{B_0} = 1 \text{ cm}^2 \text{ yr}^{-1}$ , mixed layer depth = 32 cm,  $f = 0.6$ , and  $T = 20 \text{ yr}$  (Table 2). The fits can be improved appreciably by allowing for an additional rapid mixing layer ( $D_{B_0} = 50 \text{ cm}^2 \text{ yr}^{-1}$  and mixed layer depth = 3 cm) in the sediment surface (Fig. 6I,J; Table 2). Lower-Bay sediments are subject to strong tidal currents, and sediment resuspension in this region of the estuary is common (Colman et al. 1988). However, removing 10 cm of sediment would require a major natural or artificial (e.g., dredging) disturbance. It is possible that more frequent but less powerful erosion events occurred. Although we did not simulate this scenario, we expect that the xs  $^{210}\text{Pb}$  and  $^{239,240}\text{Pu}$  profiles generated by frequent minor episodes of erosion would be equivalent to a slower net sedimentation rate. On the basis of the result of simulations with decreased sedimentation rate, those frequent minor erosional events would have to occur after 1963 (Pu peak) in order to reconcile the xs  $^{210}\text{Pb}$  and  $^{239,240}\text{Pu}$  profiles.

When an episodic deposition is applied, we could not find a set of parameters that would generate reasonable fits for both xs  $^{210}\text{Pb}$  and  $^{239,240}\text{Pu}$  profiles. Parameters that yield good fit for xs  $^{210}\text{Pb}$  predict  $^{239,240}\text{Pu}$  peak and penetration depth much deeper than observed in data.

Our simulations at the lower-Bay site show that recent changes in a previously steady-state regime (reduced sedimentation rate after 1965 and/or erosion) could explain the observed profiles of xs  $^{210}\text{Pb}$  and  $^{239,240}\text{Pu}$ . Although we lack the evidence needed to determine which, if either, of these changes is more plausible, this example again illustrates the utility of our model for exploring nonsteady processes of sediment transport.

## Summary and conclusions

Natural xs  $^{210}\text{Pb}$  and weapon-fallout  $^{239,240}\text{Pu}$  (or  $^{137}\text{Cs}$ ) remain the best tracers for modern ( $\sim 100$ -yr) chronology in muddy estuarine sediments. As others have noted, depth profiles of these tracers can frequently be interpreted with very simple steady-state models, yielding reasonable constraints on rates of sedimentation and rates and depths of bioturbation. Failure of such simple models, as applied to tracer data from cores collected in Chesapeake Bay, impelled us to develop a numerical model.

Our model implements features from previous numerical models, but it differs from them in several respects. Most importantly, when steady-state models are inadequate, we explicitly simulate time-dependent sedimentation. In addition, we optimize model parameters to simultaneously fit both chronologic tracers (xs  $^{210}\text{Pb}$  and  $^{239,240}\text{Pu}$ ). For the cases we have considered, this goodness-of-fit criterion led rapidly to reasonable values of model parameters. Success with our approach requires high-resolution tracer data and may require supporting data (e.g., sediment chemistry or flood history). Where supporting data are lacking or ambiguous, the model can identify plausible nonsteady scenarios that could explain the tracer data.

Our estimates of rates of sedimentation and bioturbation in Chesapeake Bay generally conform to patterns in those

parameters which have been previously published (Officer et al. 1984). Steady-state sedimentation was most rapid at our upper-Bay site and least rapid at the mid-Bay site. Previous estimates of mixing rates and mixed-layer depths are highly variable but have been interpreted as indicating a trend from  $D_{B_0} = 0$  at the Bay head to  $D_{B_0} \rightarrow \infty$  in the lower Bay (Officer et al. 1984). Our simulations require mixing of surface sediments at all three sites, and our best values for  $D_{B_0}$  span a considerably narrower range ( $10\text{--}50 \text{ cm}^2 \text{ yr}^{-1}$ ). Our highest value applies to our lower-Bay core, but only the top  $\sim 3$  cm was mixed at this high rate. Only our lower-Bay core required a second, slowly mixed layer, extending, in this case, to  $\sim 30$  cm. Mixed-layer depths were 10 cm or less at upper-Bay and mid-Bay sites.

At our upper-Bay and lower-Bay sites, sediment mixing alone could not explain the gradual decrease in  $^{239,240}\text{Pu}$  between the buried maximum and the sediment-water interface. Thus atmospheric deposition was augmented by a time-delayed input from elsewhere in Chesapeake Bay or its watershed. This time-delayed input accounted for 40%–50% of the  $^{239,240}\text{Pu}$  inventory in the upper-Bay and lower-Bay cores.

Much has been written concerning the relative merits of the CIC (constant initial concentration) and CRS (constant rate of supply) models for deposition of xs  $^{210}\text{Pb}$  (Appleby and Oldfield 1992). For cores in which sedimentation rate has varied, our model fits the relationship between the sedimentation rate and the flux of xs  $^{210}\text{Pb}$  through an adjustable parameter,  $P_{\text{pb}}$ . Our clearest example, the upper-Bay core, shows that this relationship varies with sedimentation rate. The flood-borne  $^{210}\text{Pb}$  flux fell between the CIC and CRS models, whereas the post-flood  $^{210}\text{Pb}$  flux was closely proportional to sediment flux.

A model that includes nonsteady sedimentation is necessarily more complex than a steady-state model. For a first-order approximation of sediment-transport parameters based on tracer data of low resolution a steady-state model may still be the best choice. Where a need for greater chronological detail justifies acquisition of high-resolution data, our model can yield improved chronologic precision and greater insight into processes of sedimentation/erosion.

## References

- ANDERSON, R. F., AND A. P. FLEER. 1982. Determination of natural actinides and plutonium in marine particulate material. *Anal. Chem.* **54**: 1142–1147.
- APPLEBY, P. G., AND F. OLDFIELD. 1978. The calculation of lead-210 dates assuming a constant rate of supply of unsupported  $^{210}\text{Pb}$  to the sediment. *Catena* **5**:1–8.
- , AND ———. 1992. Application of lead-210 to sedimentation studies, p. 731–778. *In* M. Ivanovich and R. S. Harmon [eds.], *Uranium-series disequilibrium: Applications to earth, marine, and environmental sciences*. Oxford.
- BENNINGER, L. K. 1979.  $^{210}\text{Pb}$  balance in Long Island Sound. *Geochim. Cosmochim. Acta.* **42**: 1165–1174.
- , R. C. ALLER, J. K. COCHRAN, AND K. K. TUREKIAN. 1979. Effects of biological sediment mixing on the  $^{210}\text{Pb}$  chronology and trace metal distribution in a Long Island Sound sediment core. *Earth Planet. Sci. Lett.* **43**: 241–259.
- , AND R. E. DODGE. 1986. Fallout plutonium and natural

- radionuclides in annual bands of the coral *Montastrea annularis*, St. Croix, U.S. Virgin Islands. *Geochim. Cosmochim. Acta.* **50**:2785–2797.
- , AND J. T. WELLS. 1993. Sources of sediment to the Neuse River estuary, North Carolina. *Mar. Chem.* **43**: 137–156.
- BOUDREAU, B. P., AND B. R. RUDDICK. 1991. On a reactive continuum representation of organic matter diagenesis. *Am. J. Sci.* **291**: 507–538.
- CHRISTENSEN, E. R., AND P. K. BHUNIA. 1986. Modeling radio tracers in sediments: Comparison with observations in Lake Huron and Michigan. *J. Geophys. Res.* **91**: 8559–8571.
- COLMAN, S. M., C. R. BERQUIST JR., AND C. H. HOBBS III. 1988. Structure, age and origin of the bay-mouth shoal deposits, Chesapeake Bay, Virginia. *Mar. Geol.* **83**:95–113
- COOPER S. R., AND G. S. BRUSH. 1991. Long-term history of Chesapeake Bay anoxia. *Science* **254**:992–996.
- CORNWELL, J. C., D. J. CONLEY, M. OWENS, AND J. C. STEVENSON. 1996. A sediment chronology of the eutrophication of Chesapeake Bay. *Estuaries* **19**: 488–499.
- CRONIN, T., AND OTHERS. 1999. Interdisciplinary environmental project probes Chesapeake Bay down to the core. *EOS* **80**: 237–244.
- DIBB, J. E., AND D. L. RICE. 1989. Temporal and spatial distribution of beryllium-7 in the sediments of Chesapeake Bay. *Estuar. Coast. Shelf Sci.* **28**: 395–406.
- DONOGHUE, J. F. 1990. Trends in Chesapeake Bay sedimentation rates during the late Holocene. *Quat. Res.* **34**: 33–46.
- GLADNEY, E. S., AND I. ROELANDTS. 1988. 1987 compilation of elemental concentration data for USGS BHVO-1, QLO-1, RGM-1, SCO-1, SDC-1, SGR-1 and STM-1. *Geostand. Newslett.* **12**:253–362.
- GOLDBERG, E. D., AND OTHERS. 1978. A pollution history of Chesapeake Bay. *Geochim. Cosmochim. Acta.* **42**:1413–1425.
- GRAUSTEIN, W. C., AND K. K. TUREKIAN. 1986. <sup>210</sup>Pb and <sup>137</sup>Cs in air and soils measure the rate and vertical profile of aerosol scavenging. *J. Geophys. Res.* **91**: 14355–14366.
- GROSS, M. G., M. KARWEIT, W. B. CRONIN, AND J. R. SCHUBEL. 1978. Suspended sediment discharge of the Susquehanna River to northern Chesapeake Bay, 1966 to 1976. *Estuaries* **1**: 106–110.
- HARDY, E. P., P. W. KREY, AND H. L. VOLCHOK. 1973. Global inventory and distribution of fallout plutonium. *Nature* **241**: 444–445.
- HASL. 1977. Final tabulation of monthly <sup>90</sup>Sr fallout data: 1954–1976. Health and Safety Laboratory Environmental Quarterly, Report No. HASL-329. Energy Research and Development Administration.
- HELZ, G. R., G. H. SETLOCK, A. Y. CANTILLO, AND W. S. MOORE. 1985/86. Processes controlling the regional distribution of <sup>210</sup>Pb, <sup>226</sup>Ra and anthropogenic zinc in estuarine sediments. *Earth Planet. Sci. Lett.* **76**: 23–34.
- HIRSCHBERG, D. J., AND J. R. SCHUBEL. 1979. Recent geochemical history of flood deposits in the northern Chesapeake Bay. *Estuar. Coast. Mar. Sci.* **9**: 771–784.
- IMBODEN, D. M., AND M. STILLER. 1982. The influence of Radon diffusion on the <sup>210</sup>Pb distribution in sediments. *J. Geophys. Res.* **87**:557–565.
- KEY, R. M., N. L. GUINASSO JR., AND D. R. SCHINK. 1979. Emanation of radon-222 from marine sediments. *Mar. Chem.* **7**: 221–250.
- KLEIN, E. M., C. H. LANGMUIR, AND H. STAUDIGEL. 1991. Geochemistry of basalts from the Southeast Indian Ridge, 115°E–138°E. *J. Geophys. Res.* **96**: 2089–2107.
- KRESSIN, I. K. 1977. Electrodeposition of plutonium and americium for high resolution alpha spectrometry. *Anal. Chem.* **49**: 842–845.
- LARSEN, R. J. 1985. Worldwide deposition of <sup>90</sup>Sr through 1983. U.S. Department of Energy Report EML-444. Environmental Laboratory, U.S. Dept. of Energy, New York.
- LYNCH, D. R., AND C. B. OFFICER. 1984. Nonlinear parameter estimation for sediment cores. *Chem. Geol.* **44**: 203–225.
- MARTENS, C. S., G. W. KIPPHUT, AND J. V. KLUMP. 1980. Sediment-water chemical exchange in the coastal zone traced by in situ radon-222 flux measurements. *Science* **208**:285–287.
- MCLEAN, R. I., J. K. SUMMERS, C. R. OLSEN, S. L. DOMOTOR, I. L. LARSEN, AND H. WILSON. 1991. Sediment accumulation rates in Conowingo Reservoir as determined by man-made and natural radionuclides. *Estuaries* **14**: 148–156.
- MEADE, R. H. 1982. Sources, sinks, and storage of river sediment in the Atlantic drainage of the United States. *J. Geol.* **90**: 235–252.
- MULSOV, S., B. P. BOUDREAU, AND J. N. SMITH. 1998. Bioturbation and porosity gradients. *Limnol. Oceanogr.* **43**:1–9.
- OFFICER, C. B. 1982. Mixing sedimentation rates and age dating for sediment cores. *Mar. Geol.* **46**: 261–278.
- , AND D. R. LYNCH. 1982. Interpretation procedures for the determination of sediment parameters from time-dependent flux inputs. *Earth Planet. Sci. Lett.* **61**:55–62.
- , G. H. LYNCH, G. H. SETLOCK, AND G. R. HELZ. 1984. Recent sedimentation rates in Chesapeake Bay, p. 131–157. *In* V. S. Kennedy [ed.], *The estuary as a filter*. Academic.
- ROBBINS, J. A. 1986. A model for particle-selective transport of tracers in sediments with conveyor belt deposit feeders. *J. Geophys. Res.* **91**: 8542–8558.
- , B. J. EADIE, AND D. N. EDGINGTON. 1998. Spatially variable, first-order time-averaging of <sup>137</sup>Cs fluxes to sediments in Lake Michigan as revealed by long-term changes in activities of benthic trap samples and sediments. *EOS Trans. Am. Geophys. Union* **79**: OS21P–10.
- , AND OTHERS. 2000. Time-averaged fluxes of lead and fallout radionuclides to sediments in Florida Bay. *J. Geophys. Res.* **105**: 28805–28821.
- SANTSCHI, P. H., Y.-H. LI, AND J. BELL. 1979. Natural radionuclides in the water of Narragansett Bay. *Earth Planet. Sci. Lett.* **45**: 201–213.
- SCHUBEL, J. R. 1977. Effect of Agnes on the suspended sediment of the Chesapeake Bay and contiguous shelf waters, p. 179–187. *In* E. P. Ruzecki et al. [eds.], *The effects of Tropical Storm Agnes on the Chesapeake Bay estuarine system*. Johns Hopkins Univ. Press.
- , AND H. H. CARTER. 1977. Suspended sediment budget for Chesapeake Bay, p. 48–62. *In* M. Wiley [ed.], *Estuarine processes, vol. II: Circulation sediments, and transfer of material in the estuary*. Academic.
- , AND C. F. ZABAWA. 1977. Agnes in the geological record of the upper Chesapeake Bay, p. 240–250. *In* E. P. Ruzecki et al. [eds.], *The effects of Tropical Storm Agnes on the Chesapeake Bay estuarine system*. Johns Hopkins Univ. Press.
- SEWELL, G. 2000. Finite differences, finite elements and PDE2D. Self-published. P.O. Box 12141, El Paso, TX 79913.
- SHAPIRO, L. 1975. Rapid analysis of silicate, carbonate, and phosphate rocks. *Geol. Surv. Bull.* 1401.
- SUGAI S. F., M. J. ALPERIN, AND W. S. REEBURGH. 1994. Episodic deposition and <sup>137</sup>Cs immobility in Skan Bay sediments: A ten-year <sup>210</sup>Pb and <sup>137</sup>Cs time series. *Mar. Geol.* **116**: 351–372.
- ZIMMERMAN, A. R., AND E. A. CANUEL. 2000. A geochemical record of eutrophication and anoxia in Chesapeake Bay sediments: Anthropogenic influence on organic matter composition. *Mar. Chem.* **69**: 117–137.

Received: 16 May 2000  
 Accepted: 17 April 2001  
 Amended: 26 April 2001